Available online at www.sciencedirect.com
SCIENCE DIRECT
Journal of Crystal Growth 291 (2006) 334–339
JOURNAL OF CRYSTAL GROWTH
www.elsevier.com/locate/jcrysgro

Synthesis of well-aligned ZnO nanorod arrays with high optical property via a low-temperature solution method

Ming Wang*, Chang-Hui Ye, Ye Zhang, Guo-Min Hua, Hui-Xin Wang, Ming-Guang Kong, Li-De Zhang

Key Laboratory of Materials Physics, Institute of Solid State Physics, Chinese Academy of Science, Hefei, Anhui 230031, PR China

Received 8 February 2006; received in revised form 3 March 2006; accepted 9 March 2006
Communicated by K. Nakajima

Abstract

Well-aligned ZnO nanorod arrays on Si substrate were synthesized based on a solution method. The scanning electron microscope, X-ray diffraction pattern and Raman spectrum show that the nanorods are vertically aligned to Si substrate following a *c*-axis one-dimensional growth direction. The photoluminescence (PL) spectra exhibit a strong ultraviolet emission and a broad weak green emission. The high-resolution transmission electron microscope, energy dispersive X-ray spectroscopy and PL spectra reveal that ZnO nanorods are high crystalline with the low density of defects. The origin of the green emission was investigated through varying post-treated conditions and it can be attributed to the oxygen vacancies (V_O). The growth mechanism was also discussed.

PACS: 81.05.Hd; 81.16.Be; 78.67.Lt

Keywords: A1. Characterization; A1. Nanostructure; A3. Liquid phase epitaxy; B1. Nanomaterials

1. Introduction

High-quality wide-band gap semiconductor nanostructure arrays are promising functional components for the next-generation nanometer-scale photonic and electronic devices [1,2]. Among wide-band gap semiconductor materials, ZnO is one of the most appealing candidates due to its large exciton binding energy at room temperature, excellent chemical and thermal stability and biocompatibility. Recently, the observation of room-temperature ultraviolet lasing from ZnO nanorod arrays [2] has stimulated tremendous effort on the synthesis of high-quality ZnO nanorod arrays. The methods include molecular beam epitaxy (MBE) [3], metal-organic chemical vapor deposition (MOCVD) [4], catalyst or anodic aluminum oxide (AAO) template-assisted routes [5,6], epitaxial electrodeposition [7] and aqueous solution growth (ASG) [8,9]. Synthesis of highly oriented nanostructure arrays is of crucial importance for the development of novel devices. Comparing with above-mentioned various synthetic methods, the approach to the rational fabrication of ZnO nanorod arrays based on ASG, is the most promising technique owing to its large-scale, low-cost, environmental-benign and mild-temperatures advantages.

The photoluminescence (PL) spectra of ZnO usually exhibit ultraviolet (UV) and visible bands. The UV band was identified in terms of free and bound exciton complexes and the phonon replicas [10]. The visible emission is mainly related to deep-level emissions introduced by some defects, such as oxygen vacancies (V_O), zinc vacancies (V_{Zn}), zinc interstitials (Zn_i) and anti-site of O_{Zn} [11,12]. Up to now, the origin of the green emission is still a matter of debate, partly because of its sensitivity on the sample preparation conditions. ZnO nanorods synthesized through vapor deposition [13] usually exhibit strong visible emission, which indicate high density of defects in the ZnO. By lowering the synthesis temperature [14], the visible

*Corresponding author. Tel.: +86 551 5591420; fax: +86 551 5591434.
E-mail address: mwang@issp.ac.cn (M. Wang).

0022-0248/$ - see front matter © 2006 Elsevier B.V. All rights reserved.
doi:10.1016/j.jcrysgro.2006.03.033

emission band reduced. Thus the synthesis temperature plays an important role in determining the optical property of ZnO. However, in some previous reports [15,16], the ZnO nanorods synthesized through low temperature (below 100 °C) solution method exhibit strong defect-related emission. This is difficult to explain from the thermodynamic viewpoint. In this paper, we adopted the well-established route reported in Ref. [15] to synthesise well-aligned ZnO nanorod arrays grown on the Si substrate. The PL result shows the ZnO nanorod arrays possess high optical property with low density of defect. The origin of the visible emission was also investigated.

2. Experiment

The fabrication procedure consists of two steps: (a) preparation of seed-layer, (b) growth of nanorod arrays. In the first step, 0.01 M as-prepared ZnO nanocrystals were spin coated on the Si substrate for several times. ZnO nanocrystals were prepared according to the previously reported method [17]. Before coating, Si (1 0 0) wafers were cleaned with acetone in an ultrasonic bath and etched by piranha solution (2:1 mixture of concentrated H_2SO_4/30%H_2O_2). And then, the seed-layer wafers were placed in a sealed bottle containing of zinc nitrate hydrate (0.01–0.1 M) and hexamethylenetetramine (0.01–0.1 M) for 3–6 h at 75 °C. Finally the samples were rinsed with deionized water for several times and dried at 60 °C for several hours before characterization.

The structure and morphology were characterized by means of X-ray diffraction pattern (XRD) (Philips X'Pert Pro diffractometer with Cu KαRadiation), field-emission scanning electron microscope (FE-SEM, FEI, Sirion), high-resolution transmission electron microscope (HRTEM, JEOL-2010). The composition was determined by energy dispersive X-ray spectroscopy (EDS, Inca Oxford, attached to the FE-SEM). The PL (excited with the 325 nm He–Cd laser) and Raman spectra (excited with the 514.5 nm Ar^+ laser) were recorded by the LABRAM-HR spectrometer (Jobin–Yvon). The seed-layer surface was observed by atomic force microscopy.

3. Results and discussion

3.1. Structure and morphology

Fig. 1 shows scanning electron microscope (SEM) images of the ZnO nanorod arrays grown on Si substrate. The low-magnification image shows a large area uniform film-like material deposited on the substrate (Fig. 1(a)).

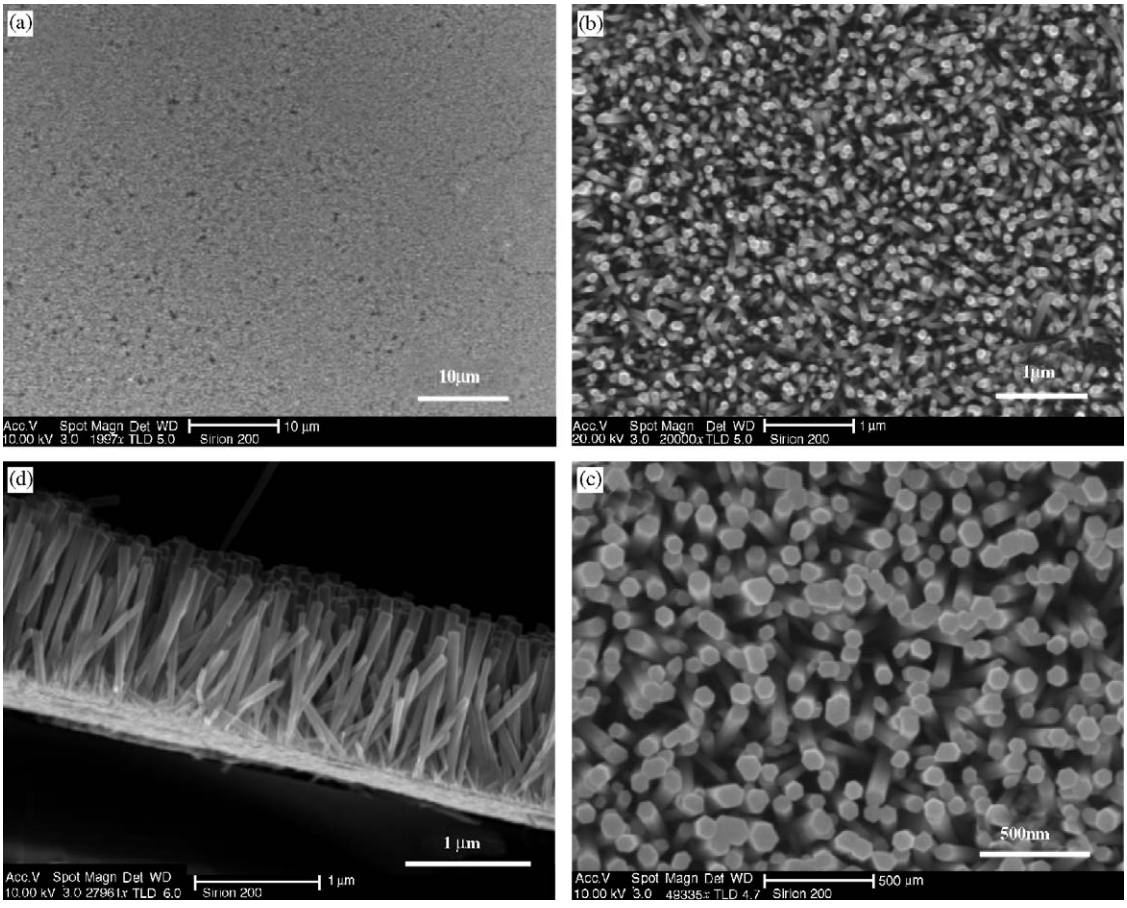

Fig. 1. FE-SEM images of the well-aligned ZnO nanorod arrays on Si wafer. (a) Large-scale and low magnification, (b) and (c) fine structure of the nanorods under high magnification, (d) cross-sectional view.

From the high-magnification images (Figs. 1(b) and (c)), it can be seen that a high density of ZnO nanorods with well-defined hexagonal facets (0 0 1) were grown vertically on the substrate. The nanorods have a narrow size distribution centered at about 100 nm in diameter. The cross-sectional view (Fig. 1(d)) of the nanorod arrays demonstrated that the ZnO nanorods grew vertically with identical length about 1.2 μm. The diameters and length of the nanorods can be tailored by controlling the growth parameters such as growth time, temperature, and zinc salt concentration.

Fig. 2(a) shows the corresponding XRD pattern of the ZnO nanorod arrays grown on the Si substrate. The intensity of the (0 0 2) peak is very strong compared with that of the other peaks such as (1 0 0) and (1 1 0). The result indicates the ZnO nanorod arrays are highly aligned perpendicular to the Si substrate with *c*-axial growth direction. The individual single nanorod was characterized using a high-resolution transmission electron microscopy (HRTEM). The images illustrate that the ZnO nanorod has high-quality single-crystal structure with smooth surface and follows [0 0 1] growth direction (Fig. 2(b)). This result is consistent with that confirmed by SEM images and XRD pattern. The corresponding selected area electron diffraction further proves the single-crystalline property of ZnO nanorod and their [0 0 1] growth direction (inset of Fig. 2(b)). Fig. 2(c) shows the chemical composition of the nanorods determined by EDS. Only oxygen, zinc, and silicon were detected. The silicon element comes from the substrate. This confirms that the nanorods are primarily ZnO.

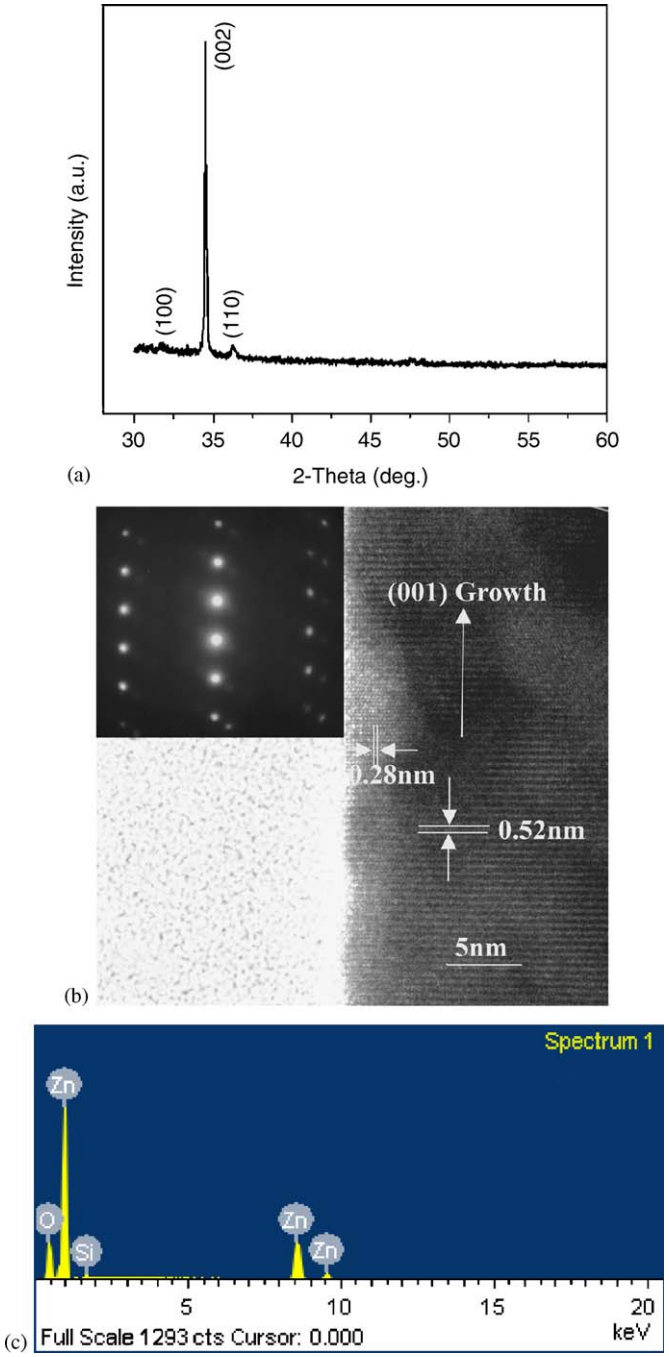

Fig. 2. (a) XRD pattern of the ZnO nanorod arrays, (b) HRTEM image of a single ZnO nanorod and the corresponding selected area electron diffraction pattern (inset), (c) Energy dispersed X-ray spectroscopy (EDS) of the ZnO nanorod arrays.

3.2. Raman spectrum

Raman scattering is an effective method to investigate the crystallization, structure and defects in the nanostructure materials. Wurtzite ZnO belongs to the C_{6v}^4 space group with two formula units per primitive cell. Based on the group theory analysis, at the Γ point of the Brillouin zone, the $A_1+E_1+2E_2$ modes are Raman active [18]. In this experiment, the incident light is normal to the substrate, namely, the incident light is parallel to the *c*-axis of the nanorods and the Raman signal was recorded in the backscattering geometry. In this configuration, only A_1 (LO) and E_2 modes are allowed and the other modes are forbidden according to the Raman selection rules [19,20]. The Raman spectrum of the ZnO nanorod arrays was shown in Fig. 3. As expected, only the E_2 (high) mode at 438 cm^{-1} and A_1 (LO) mode at 575 cm^{-1} were observed, which further confirms that the ZnO nanorod arrays are highly *c*-axis oriented. The peaks at 301, 520 and 617 cm^{-1} originate from the Si substrate.

3.3. PL spectra

The optical properties of the ZnO nanorods were investigated by PL spectroscopy excited with the 325 nm He–Cd laser. The exciting power intensity was about 2 $kW\,cm^{-2}$. Fig. 4 show the room-temperature PL spectra of the as-grown sample and the post-treated samples. A dominant emission peak is observed at about 380 nm for the three samples, which can be attributed to the recombination of the free excitons or the near band edge emission of the wide band-gap ZnO [3,21]. Obviously, after being annealed in air (line b) and in hydrogen ambient (line c), the intensity of the UV emission increased and its peak position red shifted from 375 to 385 nm, which indicates

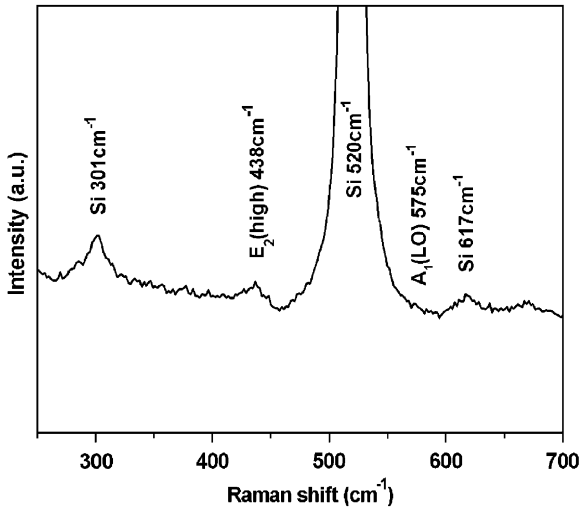

Fig. 3. Raman spectrum of the ZnO nanorod arrays grown on the Si substrate.

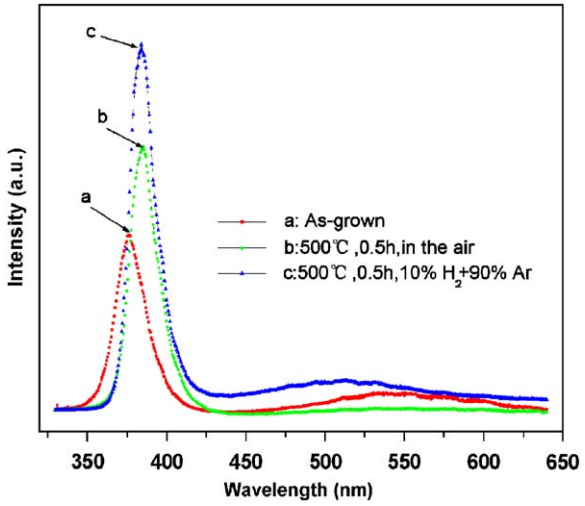

Fig. 4. Room temperature PL spectra of the ZnO nanorod arrays of the as-grown and post-treated samples.

that the annealing treatment reduces the nonradiative action and improves the crystal quality of the nanorods [22]. Furthermore, the full-width at half-maximum (FWHM) of the UV emission is estimated to be 110 meV, a little smaller than the value (120 meV) obtained from other synthesis methods [23,24]. This narrow FWHM indicates the high crystal quality of the ZnO naorod arrays with narrow size distribution. In addition to the UV emission, a weak and broad emission centered at 530 nm also can be observed from the as-grown sample. After annealing in the air at 500 °C for half an hour, this peak completely disappeared, which indicate that the defects in the ZnO are low and can be eliminated easily by a simple heat treatment. The green emission can be attributed to the V_O and Zn_i in the ZnO nanorods. In order to confirm this assignment, we annealed the sample in the hydrogen ambient. As shown in line c, the green band is a little increased. This result is consistent with the finding reported by Cocivera [25] that the oxygen vacancies increase under reductive annealing gas.

To distinguish PL bands caused by zinc interstitials (Zn_i) and oxygen vacancies (V_O) in experiments are usually difficult. Recently, Kohan et al. [26] and Van de Walle [27] calculated the formation energies and electronic structure of native point defects in ZnO theoretically. The concentration of defects in a crystal depends upon its formation energy E^f in the following form:

$$c = N_{\text{sites}} \exp\left(-\frac{E^f}{k_B T}\right), \tag{1}$$

where N_{sites} stand for the concentration of sites where the defects can occupied. E^f is related to chemical potentials of zinc, oxygen and zinc oxide which depend on the growth conditions. The formation energy of a point defect in a charge state q can be described as:

$$E^f(q) = E^{\text{tot}}(q) - n_{Zn}\mu_{Zn} - n_O\mu_O - qE_F, \tag{2}$$

where $E^{\text{tot}}(q)$ means the total energy of a system containing n_{Zn} and n_O zinc and oxygen atoms, μ_{Zn} and μ_o are the chemical potentials for zinc and oxygen, and E_F is the Fermi energy. Their calculation result shows that oxygen and zinc vacancies are the two most common defects in ZnO. In zinc-rich conditions, the oxygen vacancies (V_O) have lower formation energy (1.2 eV) than the zinc interstitials (Zn_i) and will dominate in the defect, and in oxygen-rich conditions, zinc vacancies (V_{Zn}) should dominate. In this aqueous growth condition, Zn comes from the zinc salts and the O comes from the OH^-. This aqueous system can be classified as Zn-rich conditions due to the high solubility of the zinc salts. Therefore, deduced from our PL spectra result, only the low density of oxygen vacancies (V_O) is responsible for the green emission. The zinc interstitials (Zn_i) and zinc vacancies (V_{Zn}) could be excluded in our samples. Otherwise, from the above Eq. (1), the growth temperature also plays an important role in determining the concentration of defects. Comparing the synthesis temperature in our experiments with the vapor transportation deposition, the defect concentration should be reduced. Our PL results are consistent with the thermodynamic principles. The low growth temperature results in strong UV emission and weak green emission owing to the low density of defects in the ZnO nanorods.

3.4. Growth mechanism

The growth of oxide nanorods from aqueous solution involves controlled heterogenous nucleation and homogeneous nucleation on the substrate [28]. In this chemical solution, the hexamethylenetetramine decomposed to formaldehyde and ammonia, which act as a pH buffer to regulate the pH value of the solution and supply of OH- slowly [29,30]. Through the whole experiment, the pH

value keeps about 6–7. The main chemical process can be described as

$$(CH_2)_6N_4 + 6H_2O \rightarrow 6HCHO + 4NH_3, \quad (3)$$

$$NH_3 + H_2O \rightarrow NH_4^+ + OH^-, \quad (4)$$

$$\left(2OH^- + Zn^{2+} \rightarrow Zn(OH)_2\right), \quad (5)$$

$$Zn(OH)_2 \rightarrow ZnO + H_2O. \quad (6)$$

The most stable crystal of ZnO is wurtzite structure consisting of polar (0 0 0 1), (0 0 0 $\bar{1}$) planes and non-polar (1 0 0 0) planes with C_{6v} symmetry. Due to its anisotropic crystal structure, the *c*-axis is the most preferred growth orientation, and the velocities of growth under hydrothermal conditions are $V[0\,0\,0\,1] > V[0\,1\,1\,0] > V[1\,0\,0\,0]$ [31]. Because of the polar nature of positively or negatively charged ZnO surface, the surface attracted opposite charged ions on it and reacted to form ZnO nanorods owing to its anisotropic growth character [32]. The undercoat of ZnO nanoparticles on the substrate plays an very important role in achieving high density of uniform ZnO nanorods arrays. The ZnO nanocrystals on the substrate were observed by atomic force microscopy. As shown in Fig. 5, a very uniform nanocrystals adhering to the substrate can be observed, which served as the nucleation centers. Without the seed layer, there are seldom nanorods randomly distributed on the bared substrate (see Fig. 6(a)). In the growth process, we find the solution became turbid after 1 h. The initial growth stage plays a very important role in obtaining the high quality of ZnO nanorod arrays. From the thermodynamic view, the heterogeneous nucleation is more favorable than homogeneous nucleation due to its low supersaturation. Thus the whole growth process can be divided into two parts: the hetero geneous nucleation-dominant and the homogeneous nucleation dominant process. Aim to test this assignment, the seed-coated substrate was put into the bottle after the solution became turbid. As shown in Fig. 6(b), the ZnO nanorods are large and just randomly distributed on the substrate. This shows that the nanorods are formed through the homogeneous nucleation. The growth time, concentration and temperature just only affect the ZnO nanorod size and length.

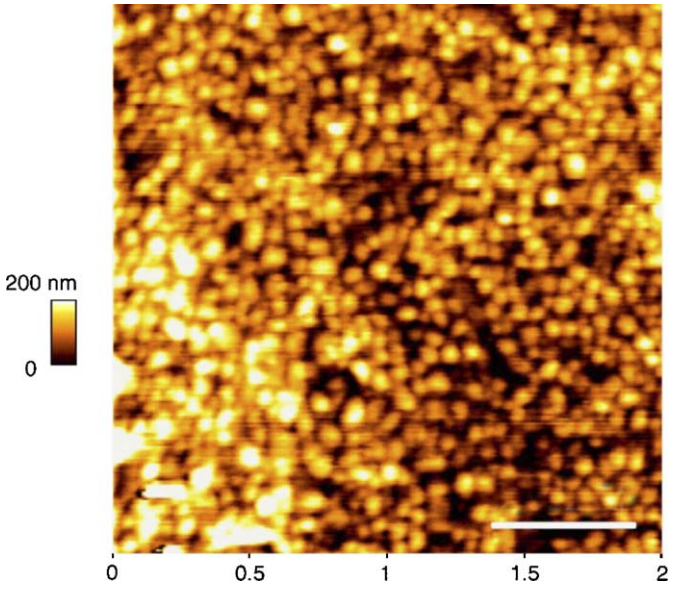

Fig. 5. AFM image of the seed-coated Si substrate.

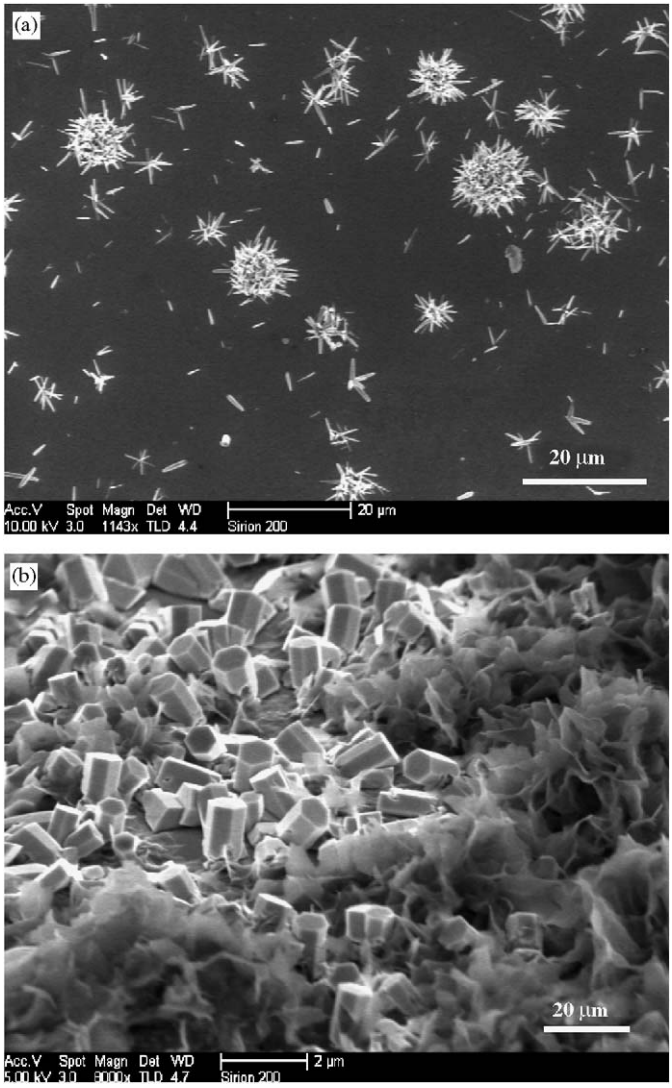

Fig. 6. FE-SEM images of (a) nanorods grown on bare Si substrate, (b) nanorods obtained from the seed-coated Si substrate when it was put into the bottle after the solution became turbid.

4. Conclusion

In summary, well-aligned ZnO nanorod arrays can be produced through a simple route based on the ASG approach. The nanorod arrays are highly *c*-axis oriented and perpendicular to the substrate with high crystalline quality. These samples exhibit strong UV emission and weak broad green emission, which indicate the high optical quality of the ZnO nanorod arrays with low density of

defects. The defect-related green emission was studied by varying the annealing conditions. The green emission is attributed to the oxygen vacancies (V_O) in the ZnO nanorods. The initial growth stage is very important in achieving the high density of ZnO nanorod arrays. These ZnO nanorod arrays have good potential application in photoelectric devices.

Acknowledgments

This work was supported by Major Research Plan of National Natural Science Foundation of China (Grant no. 90406008) and National Major Fundamental Project: Nanomaterials and Nanostructures (Grant no. 2005CB623603).

References

[1] Z.L. Wang, J. Phys.: Condens. Matter. 16 (2004) R829.
[2] M.H. Huang, S. Mao, H. Feick, H. Yan, Y. Wu, H. Kind, E. Weber, R. Russo, P. Yang, Science 292 (2001) 1897.
[3] Y. Segawa, A. Ohtomo, M. Kawasaki, H. Koinuma, Z.K. Tang, P. Yu, G.K.L. Wong, Phys. Status Solidi b 202 (1997) 669.
[4] W.I. Park, D.H. Kim, S.W. Jung, G.C. Yi, Appl. Phys. Lett. 80 (2002) 4232.
[5] M.H. Huang, S. Mao, H. Feick, H. Yan, E. Weber, P. Yang, Adv. Mater. 13 (2001) 113.
[6] Y. Li, G.W. Meng, L.D. Zhang, F. Phillipp, Appl. Phys. Lett. 76 (2000) 2011.
[7] R. Liu, A.A. Vertegel, E.W. Bohannan, T.A. Sorenson, J.A. Switzer, Chem. Mater. 13 (2001) 508.
[8] L. Vayssieres, Adv. Mater. 15 (2003) 464.
[9] Z.R. Tian, J.A. Voigt, J. Liu, B. Mckenzie, M.J. Mcdermott, M.A. Rodriguez, H. Konishi, H.F. Xu, Nat. Mater. 2 (2003) 821.
[10] S.A. Studenikin, M. Cocivera, W. Kellner, H. Pascher, J. Lumin. 91 (2000) 223.
[11] K. Vanheusden, W.L. Warren, C.H. Seager, D.R. Tallant, J.A. Voigt, B.E. Gnade, J. Appl. Phys. 79 (1996) 7983.
[12] Y.F. Chen, D.M. Bagnall, H.J. Koh, K.T. Park, K. Hiraga, Z.Q. Zhu, T. Yao, J. Appl. Phys. 84 (1998) 3912.
[13] V.A.L. Roy, A.B. Djurisic, W.K. Chan, J. Gao, H.F. Lui, C. Surya, Appl. Phys. Lett. 83 (2003) 141.
[14] J.J. Wu, S.C. Liu, Adv. Mater. 14 (2002) 215.
[15] L.E. Greene, M. Law, J. Goldberger, F. Kim, J.C. Johnson, Y. Zhang, R.J. Saykall, P. Yang, Angew. Chem. Int. Ed. 42 (2003) 3031.
[16] Q. Tang, W. Zhou, J. Shen, W. Zhang, L. Kong, Y. Qian, Chem. Commun. (2004) 712.
[17] L. Spanhel, M.A. Anderson, J. Am. Chem. Soc. 113 (1991) 1511.
[18] C.A. Arguello, D.L. Rousseau, S.P.S. Porto, Phys. Rev. 181 (1969) 1351.
[19] A. Kaschner, U. Haboeck, M. Strassburg, M. Strassburg, G. Kaczmarczyk, A. Hoffmann, C. Thomsen, A. Zeuner, H.R. Alves, D.M. Hofmann, B.K. Meyer, Appl. Phys. Lett. 80 (2002) 1909.
[20] T.C. Damen, S.P.S. Porto, B. Tell, Phys. Rev. 142 (1966) 570.
[21] J.J. Wu, S.C. Liu, Adv. Mater. 14 (2002) 215.
[22] S.T. Tan, B.J. Chen, X.W. Sun, W.J. Fan, H.S. Kwok, X.H. Zhang, S.J. Chua, J. Appl. Phys. 98 (2005) 013505.
[23] J.S. Jie, G.Z. Wang, Q.T. Wang, Y.M. Chen, X.H. Han, X.P. Wang, J.G. Hou, J. Phys. Chem. B 108 (2004) 11976.
[24] C. Geng, Y. Jiang, Y. Yao, X. Meng, J.A. Zapien, C.S. Lee, Y. Lifshitz, S.T. Lee, Adv. Funct. Mater. 14 (2004) 589.
[25] S.A. Studenikin, N. Golego, M. Cocivera, J. Appl. Phys. 84 (1998) 2287.
[26] A.F. Kohan, G. Ceder, D. Morgan, C.G. Van de Walle, Phys. Rev. B 61 (2000) 15019.
[27] C.G. Van de Walle, Physica B 308–310 (2001) 899.
[28] L. Vayssieres, K. Keis, S.-E. Lindquist, A. Hagfeldt, J. Phys. Chem. B 105 (2001) 3350.
[29] J.G. Strom Jr., H.W. Jun, J. Pharm. Sci. 69 (1980) 1261.
[30] K. Govender, D.S. Boyle, P.B. Kenway, P.O. Brien, J . Mater . Chem . 14 (2004) 2575.
[31] R.A. Laudise, A.A. Ballman, J. Phys. Chem. B 64 (1960) 688.
[32] Z.L. Wang, X.Y. Kong, Y. Ding, P. Gao, W.L. Hughes, R. Yang, Y. Zhang, Adv. Funct. Mater. 14 (2004) 943.